

## A note on the BFKL pomeron and the “hot spot” cross section

J. Bartels and H. Lotter

*II. Institut für Theoretische Physik, Universität Hamburg, Hamburg, FRG*

Received 18 March 1993; revised manuscript received 30 April 1993

Editor: P.V. Landshoff

We comment on the numerical calculation of the Lipatov pomeron in the measurement of “hot spots” in deep inelastic scattering. We illustrate that previous analytic estimates based upon the leading term in the Lipatov equation are accurate within 20%. We present evidence that numerical calculations should be done with a fixed  $\alpha_s$ . The use of a running  $\alpha_s$  appears as an unnecessary complication. We argue that at low  $Q^2$  the BFKL pomeron requires higher-order corrections.

1. Some time ago Mueller and Navelet [1] have suggested to measure, in hadron–hadron collisions at high energies, a particular configuration of jets in the final state which allows to observe, for the first time, the Balitsky–Fadin–Kuraev–Lipatov (BFKL) pomeron [2–5] in QCD. More recently, Mueller [6] reformulated this measurement for deep inelastic scattering at HERA. The idea is to identify in deep inelastic scattering (characterized by  $x_B, Q^2$ ) events with one jet in the hadronic final state which carries transverse momentum  $k_T^2 \sim Q^2$  and longitudinal momentum fraction  $x_J \gg x_B$ . This corresponds to an off-shell photon–off-shell gluon (quark) scattering process in the limit  $s/Q^2 \sim x_J/x_B \equiv 1/z \gg 1$ . If both virtualities are sufficiently large,  $\alpha_s$  is small and perturbative QCD can be used. The leading logarithmic approximation is given by the BFKL pomeron, i.e. the sum of gluon ladders between the jet-emission vertex and the coupling of gluons to the photon via a quark loop. Due to the choice  $k_T^2 \sim Q^2$  there is no evolution in transverse momentum between the emission of the jet and the interaction with the photon; that is why the BFKL pomeron applies, and not the usual Gribov–Lipatov–Altarelli–Parisi evolution [7,8]. In impact parameter space, the emission of the jet takes place close to the photon interaction vertex. Therefore, the measurement of such jets “explores the region around the photon interaction vertex”, the so-called “hot spot”. This is quite in contrast to the inclusive measurement of deep inelastic structure functions which averages over the full size of the hadron and gives no information on the spatial distribution of partons inside the hadron. The  $x_J/x_B$ -dependence of the differential cross section for such “hot spot” events depends only upon the BFKL pomeron and not the initial parton distribution  $D_P(x, k^2)$ . It is also believed that first “screening” corrections to the BFKL pomeron might become important rather soon: they should manifest themselves in a suppression of the measured cross section compared to the prediction of the BFKL pomeron. The analytic expression for these first corrections has been derived recently in ref. [9].

Analytic [10–12] and numerical [10,11] estimates of the BFKL pomeron in the “hot spot” cross section have been discussed by several groups. They all agree in the analytic formula, which, however, introduces another step of approximation (the “leading singularity” approximation to the BFKL pomeron), whereas the numerical evaluation has been done in different ways. In ref. [10] the analytic approximation was compared to a Monte Carlo simulation, based upon the usual GLAP evolution program. Although there is evidence that in the HERA region there is not much difference yet between the GLAP evolution and the BFKL-improved description, this comparison seems not really satisfactory. Moreover, a repeat of the Monte Carlo simulation based upon another routine shows quite a distinct answer [13]. The analysis in ref. [11], on the other hand, compares the analytic approximation with a computer calculation of the BFKL equation, but the latter one is done with a

running  $\alpha_s$  instead of the fixed  $\alpha_s(Q^2)$  (the derivation of the BFKL pomeron does *not* include the renormalization of  $\alpha_s$  which renders the fixed coupling momentum dependence). When replacing “by hand” the fixed coupling by the running one, the  $k_t$  integration in the BFKL equation becomes infrared divergent (whereas the original equation was finite), and one is forced to introduce an infrared cutoff. As a result, the numerical answer depends upon this cutoff, and this dependence turns out to be rather strong. In summary, both numerical estimates are unsatisfactory and require a new attempt, namely the numerical calculation of the BFKL pomeron with fixed  $\alpha_s$ .

Apart from the “hot spot” cross section, the BFKL pomeron has attracted interest also for the  $x$ -dependence of the gluon structure function [14–16]. It predicts a rather steep increase in the small- $x$  region. Numerical calculations are again plagued [11] by the dependence upon the infrared cutoff, which appears as a result of introducing the running  $\alpha_s$ . In ref. [16] this dependence turns out to be so strong that, in our opinion, it seriously raises the question whether (and how) the BFKL pomeron can be used *at all* in this context.

In this letter we present results of a new numerical calculation which, as we hope, will help to clarify both questions, the comparison of the analytic approximation to the “hot spot” cross section with the BFKL pomeron, and the use of the BFKL pomeron for the gluon structure function at low  $Q_0^2$ . We have done, for the “hot spot” cross section, a numerical analysis of the BFKL pomeron with fixed  $\alpha_s$ , and we find surprisingly good agreement with the analytic “leading singularity” approximation. In a second step we have analyzed, in our numerical calculation, which region of transverse momentum gives the dominant contribution. For the “hot spot” cross section in the HERA region (and above), at  $k_J^2, Q^2$  between 50 and 100 GeV<sup>2</sup>, the transverse momentum is concentrated in the region above 1 GeV<sup>2</sup>. This supports the expectation that the leading power in  $x_J/x_B$  becomes visible *before* the diffusion in transverse momentum has reached the dangerous infrared region. The use of the running coupling, therefore, appears as an unnecessary complication. For lower  $Q^2$ , however, the situation is very different. The dangerous infrared region  $k^2 < 1$  GeV<sup>2</sup> now becomes an essential part of the integration region, and higher-order corrections cannot be neglected.

2. The differential cross section for the “hot spot” process reads #1 [10]

$$x_J k_J^4 \frac{d^4\sigma}{dx_J dk_J^2 dx_B dy} = \frac{4\pi\alpha_{EM}^2}{Q^2} \frac{1}{2} \sum_{q,\bar{q}} e_q^2 \left[ y\Phi_1\left(\frac{x_J}{x_B}, k_J^2, Q^2\right) + \frac{1-y}{y} \frac{pq}{M^2 x_B} \Phi_2\left(\frac{x_J}{x_B}, k_J^2, Q^2\right) \right] \\ \times \frac{12\alpha_s(k_J^2)}{4\pi} \left( x_J D_{\mathbb{F}}^{\mathbb{F}}(x_J, k_J^2) + \frac{4}{9} \sum_{\mathbb{F}} [x_J D_{\mathbb{F}}^{\mathbb{F}}(x_J, k_J^2) + x_J D_{\mathbb{F}}^{\mathbb{F}}(x_J, k_J^2)] \right). \tag{1}$$

The  $\Phi_i$  are defined analogously to the canonical  $W_i$ . In the limit  $x_B/x_J \ll 1$  they are given by Lipatov ladders with a suitable coupling to the virtual photon and without external gluon propagators. The second part describes the jet-emission vertex, and the expression in square brackets contains the parton content of the proton, parametrized in terms of the structure functions.

The  $\Phi_i$  are solutions of the BFKL equation [2–4] averaged over the angle in the transverse momentum plane:

$$\frac{\partial}{\partial \log 1/z} \Phi_i\left(\frac{1}{z}, \frac{k^2}{Q^2}\right) = \frac{N_c\alpha_s}{\pi} \int_0^\infty dk'^2 \frac{k^2}{k'^2} \left[ \frac{1}{|k^2 - k'^2|} \Phi_i\left(\frac{1}{z}, \frac{k'^2}{Q^2}\right) - \left( \frac{1}{|k^2 - k'^2|} - \frac{1}{(k^4 + 4k'^4)^{1/2}} \right) \Phi_i\left(\frac{1}{z}, \frac{k^2}{Q^2}\right) \right]. \tag{2}$$

As the initial condition we take the sum of quark-box diagrams  $\Phi_{\mu\nu}^{(0)}$  [10] (quark masses are neglected):

$$\Phi_{\mu\nu}^{(0)} = -\frac{1}{2} (4I_1 + I_2), \tag{3}$$

#1 In comparison with ref. [10] slightly different definitions for the  $\Phi_i$  are used. In particular they contain no external gluon propagators.

$$\frac{pq}{M^2 x_B} \Phi_2^{(0)} = -4(3I_1 + \frac{1}{4}I_2), \tag{4}$$

$$I_1 \equiv \frac{1}{4\pi} \Phi_{\mu\nu}^{(0)} p^\mu p^\nu \frac{x_B^2}{q^2} = \frac{-1}{4\pi} \alpha_s Q^2 \int_0^1 \int_0^1 dx dy \left( \frac{Q^2 y^2 (1-y)^2}{-x(1-x)k^2 - y(1-y)Q^2} + y(1-y) \right), \tag{5}$$

$$I_2 \equiv \frac{1}{4\pi} \Phi_{\mu\nu}^{(0)} g^{\mu\nu} = \frac{-1}{4\pi} \alpha_s Q^2 \int_0^1 \int_0^1 dx dy \left( \frac{k^2 [2y(1-y) - 1 + 2x(1-x)]}{-x(1-x)k^2 - y(1-y)Q^2} \right). \tag{6}$$

We choose our evolution to start at  $z=1$  (this differs from the treatment of ref. [11] where the starting point is  $z_0=10^{-1}$ ). For the numerical solution the BFKL equation (2) is discretized in  $k^2$  (a similar method was employed in ref. [17]). This procedure leads to a system of ordinary differential equations which can be solved with a Runge-Kutta one-step method. For the discretization we introduce an upper and lower cutoff  $k_0^2/k_F^2$  and transform to the new variable  $t=\log(k^2/k_0^2)/\log(k_F^2/k_0^2)$ . The integral is approximated with the trapezium rule. The kernel in (2) is singular for  $t=t'$ . However, for  $\Phi_i$  differentiable in  $k^2$  the full integrand in (2),  $I(t, t')$ , has well-defined limits  $t' \uparrow t, t' \downarrow t$ . We put

$$I(t_1, t_1) = \lim_{t' \uparrow t_1} I(t_1, t'), \tag{7}$$

$$I(t_i, t_i) = \frac{1}{2} \left( \lim_{t' \uparrow t_i} I(t_i, t') + \lim_{t' \downarrow t_i} I(t_i, t') \right), \tag{8}$$

$$I(t_N, t_N) = \lim_{t' \uparrow t_N} I(t_N, t'). \tag{9}$$

In this way we obtain the matrix equation:

$$\frac{\partial}{\partial y} \Phi(k^2(t_i), y) = \sum_{j=1}^N K(k^2(t_i), k^2(t_j)) \Phi(k^2(t_j), y), \tag{10}$$

where  $y = \ln 1/z$ . We have tested the stability of our results against variations in  $k_0^2, k_F^2$  and  $N$ . For the calculations we use  $k_0^2 = 10^{-12} \text{ GeV}^2, k_F^2 = 10^{16} \text{ GeV}^2, N = 200$ . The functions  $\Phi_1, \Phi_2$  are calculated for different values of  $k_j^2/Q^2$  and values of  $z = x_B/x_j$  between 1 and  $10^{-6}$ . The results are compared with the approximate analytical solution of the BFKL equation [10],

$$\begin{aligned} \Phi_1 &= k^2 \sqrt{\frac{Q^2}{k^2}} \frac{1}{\sqrt{\log 1/z}} \left(\frac{1}{z}\right)^{x(0)} \exp\left(\frac{-(\log k^2/Q^2)^2}{2\chi''(0)\log 1/z}\right) \frac{A_1}{\sqrt{28N_c\alpha_s\zeta(3)}}, \\ \frac{pq}{M^2 x_B} \Phi_2 &= k^2 \sqrt{\frac{Q^2}{k^2}} \frac{1}{\sqrt{\log 1/z}} \left(\frac{1}{z}\right)^{x(0)} \exp\left(\frac{-(\log k^2/Q^2)^2}{2\chi''(0)\log 1/z}\right) \frac{A_2}{\sqrt{28N_c\alpha_s\zeta(3)}}, \end{aligned} \tag{11}$$

where

$$\chi(0) = \frac{N_c\alpha_s}{\pi} 4 \log 2, \quad \chi''(0) = \frac{N_c\alpha_s}{\pi} 28\zeta(3), \tag{12}$$

and  $A_1, A_2$  collect factors resulting from the quark-box integrals.

Numerical results for the  $\Phi_i$  at different ratios  $k_j^2/Q^2$  are shown in figs. 1 and 2, curves for the cross section in fig. 3. The solutions in figs. 1 and 2 show the characteristic power behaviour of the BFKL pomeron (straight lines in our double logarithmic plot) for  $z \sim 10^{-3}, 10^{-4}$ . In general the analytic solution overestimates the numerical one. It can further be seen that the analytic solution becomes better as the ratio  $k_j^2/Q^2$  is getting close to 1. For small  $k_j^2/Q^2$ , we are closer to the deep inelastic situation: before we reach the power behaviour of the

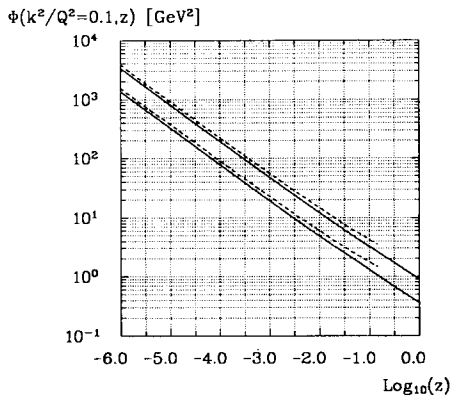


Fig. 1. Structure functions  $\Phi_1$  (lower curves) and  $\Phi_2$  (upper curves) for  $Q^2=100 \text{ GeV}^2$ ,  $k_T^2=10 \text{ GeV}^2$ , and  $10^{-6} \leq z \leq 1$ . Straight lines show numerical calculations, dashed lines represent the analytic approximation.

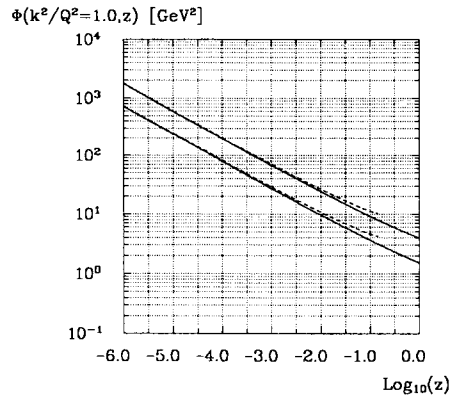


Fig. 2. Same as fig. 1 but for  $k_T^2=100 \text{ GeV}^2$ .

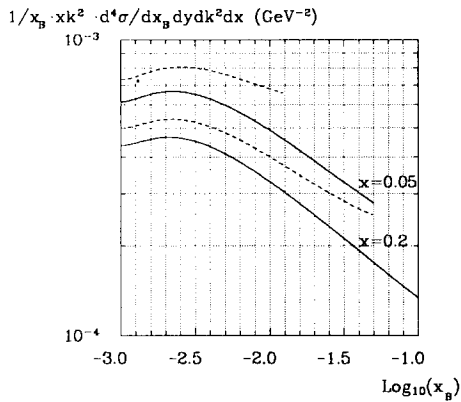


Fig. 3. Differential cross section for the “hot spot” process at HERA for different values of  $x_j Q^2$  is  $100 \text{ GeV}^2$  and  $k_T^2$  is  $50 \text{ GeV}^2$ . Dashed lines show calculations based on the analytic approximation. The number of flavours is 5, and the EHQL1 parametrization of parton distributions is used.

BFKL pomeron, there is an intermediate region in which one sees the small- $x$  behaviour

$$\sim \exp\left(\sqrt{\frac{12\alpha_s}{\pi}} \log \frac{1}{z} \log \frac{Q^2}{k^2}\right).$$

This indicates that contributions from non-leading singularities depend on  $\log k^2/Q^2$  in a more complicated way than the leading one. The differential cross section (fig. 3) shows surprisingly good agreement (within 20 percent or less) between the analytic approximation and the numerical curve, for  $z < 5 \times 10^{-2}$ . This is in agreement with what was found in ref. [10]. Clearly, for larger  $x_j$  the straight line-behaviour is better visible than for the smaller  $x$ -value.

3. Having established that our fixed-coupling version of the BFKL pomeron is not too badly approximated by the analytic formula, we now move on to the second question raised above, namely whether we better should have used the running coupling instead. As a criterion for the necessity of introducing higher-order corrections (the use of the running coupling amounts to taking into account a subset of these corrections) we study the

distribution in transverse momentum inside the BFKL equation. A strong emphasis of low momenta would indicate that a substantial part comes from a region where  $\alpha_s$  is not small, and higher-order corrections are expected to be essential.

It is well known [3] that the iteration of the BFKL kernel describes a random walk in  $\log k_\perp^2$ . Starting from some initial distribution in  $k_\perp^2$  (e.g. the quark loop in our cross section), each iteration of the BFKL kernel leads to a broadening of the  $k_\perp$ -distribution. After a sufficiently large number of steps (or for sufficiently large rapidity), the following diffusion equation holds:

$$\frac{\partial}{\partial y} \Psi(y, \xi) = \omega_0 \Psi(y, \xi) + C \frac{\partial^2}{\partial \xi^2} \Psi(y, \xi), \quad (13)$$

where

$$\Psi(y, \xi) = \frac{\Phi(k^2)}{\sqrt{k^2}}, \quad (14)$$

$$\xi = \log \frac{k^2}{Q^2}, \quad (15)$$

$$\omega_0 = \frac{N_c \alpha_s}{\pi} 4 \log 2, \quad (16)$$

$$C = \frac{N_c \alpha_s}{\pi} 14 \zeta(3). \quad (17)$$

This equation is solved by the following Green function:

$$G(y, y'; \xi, \xi') = \exp[\omega_0(y-y')] \frac{1}{[4\pi C(y-y')]^{1/2}} \exp\left(-\frac{(\xi-\xi')^2}{4C(y-y')}\right). \quad (18)$$

In particular, it follows from this equation that the mean square deviation grows linearly in rapidity:

$$\bar{\xi}^2 = \langle (\xi - \xi_{\max})^2 \rangle = 2Cy. \quad (19)$$

Fig. 4 shows a numerical calculation of the (normalized) momentum distribution  $\Psi(y, \xi)$  as function of rapidity. As initial distribution we use the result for the quark loop which (after multiplication with  $1/\sqrt{k_\perp^2}$ ) has the shape of a (slightly asymmetric) gaussian. With increasing rapidity, the distribution broadens, whereas the center stays the same. In fig. 5 we plot, as a measure for the width, the mean square deviation. For small rapidity, it is larger than the analytic prediction; for large  $y$  it reaches the value obtained from eq. (19)

4. Next we wish to study the growth of the width of the momentum distribution during the BFKL evolution. The evolution in  $\log k_\perp^2$  in fig. 5 shows that the contributing momenta rapidly enter the dangerous region  $k^2 < 1 \text{ GeV}^2$  where  $\alpha_s$  starts to feel the Landau pole and becomes large. Yet one has to keep in mind that fig. 5 shows an "unrestricted" evolution, whereas for the "hot spot" process we are interested in a sharply peaked (at  $k_\perp^2$ ) momentum distribution. This means that we have a random walk in the transverse momentum plane with the additional condition that we want to reach a particular final point. At every point of the ladder we can view the momentum distribution as a folded distribution of two evolutions originating from above and from below. It is this product distribution which gives a measure for the contributing momenta in our specific process.

For fixed rapidity gap  $y = \log 1/z$ ,  $z = 10^{-4}$ , corresponding to an optimistic HERA value, we evolve with the BFKL equation simultaneously from the quark-box and from the jet vertex. We define the product distribution  $\Psi_2(y_1, \xi) \Psi_1(y - y_1, \xi)$  in  $\xi$  as a function of  $y_1$ , where  $\Psi_2$  refers to evolution starting from the jet vertex and  $\Psi_1$  to the evolution from the quark loop. As a measure for the dominant region of integration along the ladder in the

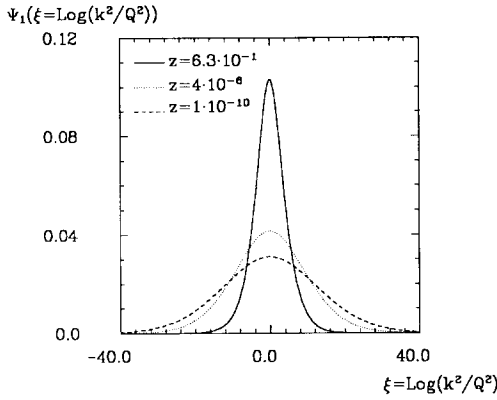


Fig. 4. The normalized distribution function  $\Psi(\xi = \log k^2/Q^2)$  calculated with the quark box as initial condition for three different values of  $z$ .

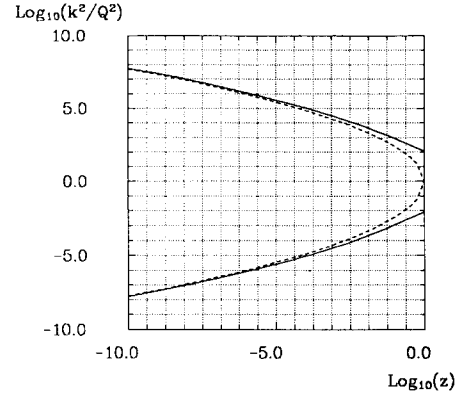


Fig. 5. Width ( $\bar{\xi}$ ) of these distributions in  $\log k^2/Q^2$  as a function of  $z$  (straight lines). The dashed lines correspond to the analytic result, eq. (19).

“hot spot” process we calculate the width of this product distribution. Formally, the dependence upon  $x_j/x_B$  of the differential cross section (1) can be written as

$$d\sigma \sim \int \frac{\delta(k_j^2 - k^2)}{[k^2]^{1/2}} \frac{\Phi(y, k^2/Q^2)}{[k^2]^{1/2}} \frac{dk^2}{k^2} \quad (20)$$

$$\equiv \Psi_2(0, \xi)^T \Psi_1(y, \xi) . \quad (21)$$

In the second line we have turned to the discretized version and replaced the integration by a summation. Numerically,  $\Psi_1(y, \xi)$  is the result of  $N$  evolution steps:

$$\Psi_1(y, \xi) = [(1 + \Delta y K)^N \otimes \Psi_0](y, \xi) . \quad (22)$$

This means that we can express the cross section equivalently in terms of our product function:

$$\Psi_2(0, \xi)^T \Psi_1(y, \xi) \quad (23)$$

$$= \Psi_2(0, \xi)^T [(1 + \Delta y K)^N \otimes \Psi_0](y, \xi) \quad (24)$$

$$= [(1 + \Delta y K)^M \otimes \Psi_2(0)](y_1, \xi)^T [(1 + \Delta y K)^{N-M} \otimes \Psi_0](y - y_1, \xi) \quad (25)$$

$$= \Psi_2(y_1, \xi)^T \Psi_1(y - y_1, \xi) . \quad (26)$$

In fig. 6 we show, for different values of  $y_1$  but fixed  $z = 10^{-4}$ , the momentum distribution, i.e. the weight of the different terms in the sum (26). The full curve belongs to the distribution at the quark loop (nearly a gaussian with center at  $Q^2 = 100 \text{ GeV}^2$ ), the dotted line corresponds to the jet vertex (sharply peaked at  $k_j^2 = 50 \text{ GeV}^2$ ) and the dashed line to a rapidity value half way in between the two extrema (almost a gaussian with the center between  $Q^2$  and  $k_j^2$ ). For a better illustration of the spread in transverse momentum we have calculated the center of the distribution ( $\xi_{\text{max}}$ ) and the root of the mean square deviation ( $\bar{\xi}$ ) as a function of  $z_1 (\xi = \log k^2/Q^2)$ . Fig. 7 shows the results, translated back into  $k^2$ . At the quark loop (left hand side, at  $z_1 \approx 10^{-4}$ ) we start with a finite width. Moving to the right, the width increases, reaches a maximum and then decreases towards zero. As the most important result, the width never reaches below  $1 \text{ GeV}^2$ . Obviously, for a smaller  $z$ -interval we expect the “cigar” to become thinner, and a change in  $Q^2$  and/or  $k_j^2$  will move the tips of the “cigar” upwards or downwards.

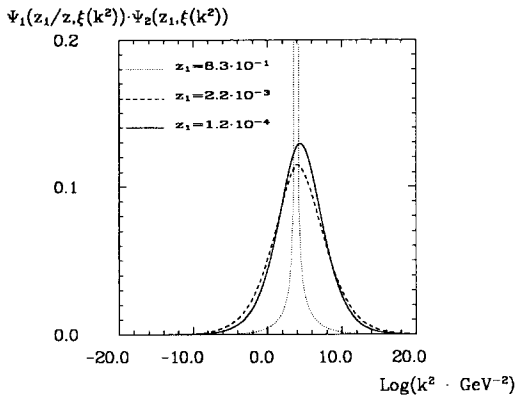


Fig. 6. Normalized product distribution  $\Psi_1 \Psi_2$  for fixed rapidity gap  $z=10^{-4}$  and three different values of  $z_1$  (corresponding to  $y_1 = \log 1/z_1$ ).

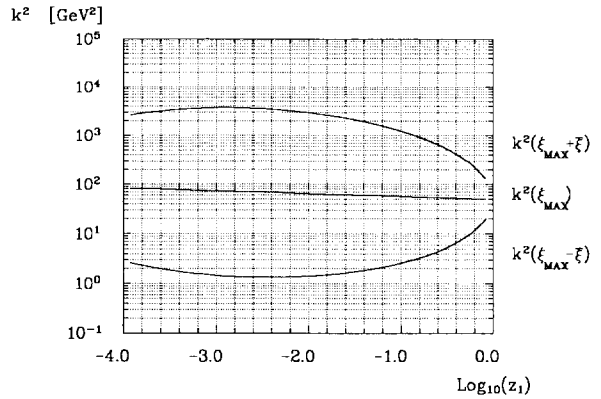


Fig. 7. Evolution of width and maximum in  $k^2$  of the product distribution  $\Psi_1(y_1, \xi) \Psi_2(y-y_1, \xi)$  as a function of  $z_1 = \exp(-y_1)$  for fixed rapidity gap  $z=10^{-4}$ .

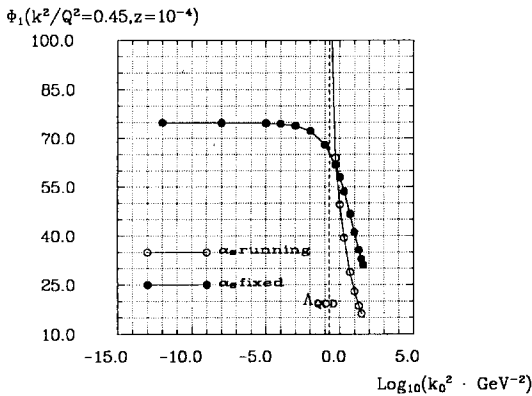


Fig. 8. The structure function  $\Phi_1(k^2/Q^2=0.45, z=10^{-4})$  from the BFKL equation, as a function of the infrared cutoff  $k_0^2$ . The dots belong to a calculation with a fixed coupling constant, the circles to a running coupling constant.

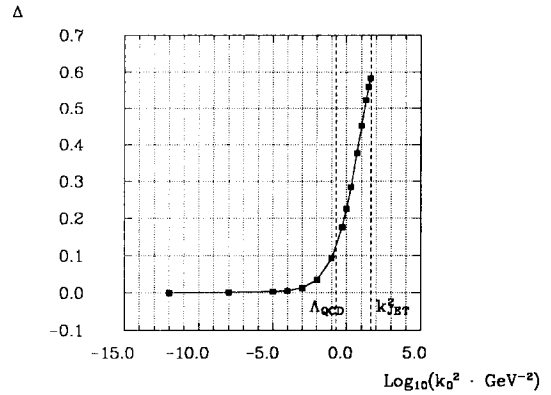


Fig. 9. Relative error  $\Delta \equiv |\Phi_{k_0^2=0} - \Phi_{k_0^2}| / \Phi_{k_0^2=0}$  of  $\Phi_1(k^2/Q^2=0.45, z=10^{-4})$  as a function of the infrared cutoff  $k_0^2$  calculated with fixed  $\alpha_s$ , with respect to the asymptotic value  $k_0^2 \rightarrow 0$ .

This result suggests the following picture. Obviously, for the “hot spot” cross section in the HERA region and  $k_T^2 \approx Q^2$  between 50 and 100  $\text{GeV}^2$ , the region below 1  $\text{GeV}^2$  is inessential, and it should not matter very much, if we introduce a cutoff, say, between 0.5 and 1  $\text{GeV}^2$ . Now we could switch from fixed to running  $\alpha_s$ . We expect the variation to be moderate, i.e. there is not much difference whether we use fixed or running  $\alpha_s$ . This, however, changes if we lower the cutoff and get into the vicinity of  $\Lambda_{\text{QCD}}$ : whereas the fixed-coupling version should remain approximately constant (we know that it has a finite limit for zero cutoff), the running-coupling version starts to grow rapidly. If, on the other hand, we increase the cutoff beyond 1  $\text{GeV}^2$ , we start to take away a part of the essential region of integration: consequently, both versions (running or fixed) should decrease and strongly depend upon the value of the cutoff.

This is all illustrated in fig. 8 where we present the  $\Phi_1$  function (at fixed  $z, Q^2$ , and  $k_T^2$ ) as a function of the

infrared cutoff. For comparison, we show both versions (fixed and running coupling). Starting from the left one sees that  $\Phi_1$  is approximately constant when fixed  $\alpha_s$  is used (dots) and  $k_0^2$  is small. When  $k_0^2$  increases the phase space gets smaller and  $\Phi_1$  decreases. For  $k_0^2 = 1 \text{ GeV}^2$  one finds a relative deviation of up to twenty percent whereas for still larger  $k_0^2$  the decrease proceeds much more rapidly. In the calculation with running coupling (circles) a similar behaviour is found for  $k_0^2$  above  $1 \text{ GeV}^2$ , whereas for lower values one soon reaches the Landau pole, and  $\Phi_1$  diverges. Fig. 9 shows the relative deviation of the cutoff version, normalized to the uncut version with fixed coupling constant. When the cutoff reaches the value of  $k_1^2$ , the relative deviation exceeds fifty percent. In summary, for a cutoff in the intermediate region the two versions do not differ too much. We feel that the use of the running coupling presents a somewhat unnecessary complication.

The fact that the curves in ref. [11] have such a strong dependence upon the cutoff is now easily understood: the calculations are done with a cutoff  $k_0^2$  between  $1 \text{ GeV}^2$  and  $4 \text{ GeV}^2$ , and all these values lie in the region well-above the "safe" interval. So they cut away more and more of the essential part of the integration region. If, on the other hand, the cutoff would have been chosen somewhat lower (but not too low), the results would have been similar to ours, i.e. close to the analytic estimate.

The situation with the influence of the infrared cutoff changes dramatically if we try to apply the BFKL pomeron to a lower  $Q^2$  scale, say, to the gluon structure function at  $4 \text{ GeV}^2$ . Let us return to fig. 7: assuming that the quark distribution at the left hand side has a similar width (remember that the quark loop has been calculated for zero quark masses and hence depends only upon the ratio  $k^2/Q^2$ ), and taking at the right hand side a distribution of a comparable shape, there is little doubt that a substantial part of the transverse momentum integration will lie below  $1 \text{ GeV}^2$  (even below  $0.1 \text{ GeV}^2$ ). Now, in our opinion, it becomes absolutely essential to take into account higher-order corrections to all elements of the BFKL equation (kernels, trajectory function), as well as contributions which unitarize the BFKL pomeron. The mere replacement of the fixed coupling by its running counterpart seems a rather poor first step. The importance of higher-order corrections or even non-perturbative effects in the BFKL pomeron has also been emphasized (although in a slightly different approach) by Landshoff et al. [18,19].

5. In this short note we tried to develop a better understanding of the BFKL evolution in the "hot spot" process. Due to its unique features mentioned in the introduction, this process offers a very appropriate environment to study QCD effects at small  $x$ , i.e. dense partonic systems in the small coupling limit.

As a first step we have calculated structure functions for this process by numerically solving the BFKL equation with fixed coupling constant. This was motivated by the fact that existing numerical studies, in our opinion, were not unambiguous. We have found that the power behaviour of the BFKL pomeron sets in for  $x_B/x_J \leq 10^{-3}$ , i.e. in a region which lies at the boarder of the HERA domain. The analytical approximate solution gives a good approximation to the behaviour of the full BFKL equation. Whether one can measure the Lipatov exponent itself clearly depends upon the corrections to the BFKL pomeron which are expected to lower the calculated curves. A numerical estimate of these corrections seems to be the most urgent task.

In a second step we tried to estimate whether the use of the fixed coupling constant in our calculations was justified. We first verified the random-walk picture in the variable  $\ln k_t^2$ , and compared our numerical calculation with the theoretical prediction. Specializing to the "hot spot" cross section we found that the region of small transverse momenta contributes very little, and we concluded that there is no need for replacing the fixed coupling by the running  $\alpha_s$ . This does not mean that the use of running  $\alpha_s$  leads to the wrong result: for our example we have shown that there is a domain of the lower momentum cutoff for which the use of fixed and running coupling constant produce almost identical results. As long as the cutoff is chosen to lie in this "safe" region one gets the correct answer. The only problem lies in the fact that, without further analysis, one does not know where this "safe" region is.

From our analysis of the relevant region of integration we also have drawn the conclusion that the use of the BFKL pomeron for the determination of the  $x$ -behaviour of the gluon distribution at lower  $Q^2$  appears, to say the least, problematic. Since the region of rather small momenta is very important,  $\alpha_s$  is no longer small and

higher-order corrections are important. This includes not only the renormalization of the coupling constant but also higher-order corrections to the BFKL kernel and, in particular, unitarity corrections.

We thank A. Mueller for a helpful suggestion.

## References

- [1] A.H. Mueller and H. Navelet, Nucl. Phys. B 282 (1987) 727.
- [2] E.A. Kuraev, L.N. Lipatov and V.S. Fadin, Sov. Phys. JETP 44 (1976) 443.
- [3] E.A. Kuraev, L.N. Lipatov and V.S. Fadin, Sov. Phys. JETP 45 (1977) 199.
- [4] Ya.Ya. Balitzky and L.N. Lipatov, Sov. J. Nucl. Phys. 28 (1987) 822.
- [5] L.N. Lipatov, Sov. Phys. JETP 63 (1986) 904.
- [6] A.H. Mueller, Nucl. Phys. B (Proc. Suppl.) 18C (1991) 125.
- [7] V.N. Gribov and L.N. Lipatov, Sov. J. Nucl. Phys. 15 (1972) 438, 675.
- [8] G. Altarelli and G. Parisi, Nucl. Phys. B 126 (1977) 297.
- [9] J. Bartels, Phys. Lett. B 298 (1993) 204.
- [10] J. Bartels, A. De Roeck and M. Loewe, Z. Phys. C 54 (1992) 635.
- [11] J. Kwiecinski, A.D. Martin and P.J. Sutton, Phys. Lett. B 287 (1992) 254; Phys. Rev. D 46 (1992) 921.
- [12] W.-K. Tang, Phys. Lett. B 278 (1991) 363.
- [13] A. De Roeck, private communication.
- [14] J. Collins and J. Kwiecinski, Nucl. Phys. B 335 (1990) 89.
- [15] J. Kwiecinski, A.D. Martin, W.J. Stirling and R.G. Roberts, Phys. Rev. D 42 (1990) 3645.
- [16] A.J. Askew, J. Kwiecinski, A.D. Martin and P.J. Sutton, Durham preprint DTP/92/78 (1992).
- [17] R.E. Hancock and D.A. Ross, Nucl. Phys. B 383 (1992) 575.
- [18] A. Donnachie and P.V. Landshoff, Nucl. Phys. B 311 (1988/89) 509.
- [19] P.V. Landshoff and O. Nachtmann, Z. Phys. C 35 (1987) 405.